Supplemental Material to "Dynamical order and superconductivity in a frustrated many-body system"

J. Tindall[1], F. Schlawin[1], M. Buzzi[2], D. Nicoletti[2], J. R. Coulthard[1],
H. Gao[1], A. Cavalleri[1,2], M. A. Sentef[2,3] and D. Jaksch[1,4]

[1]*Clarendon Laboratory, University of Oxford, Parks Road, Oxford OX1 3PU, United Kingdom*

[2] *Max Planck Institute for the Structure and Dynamics of Matter, 22761 Hamburg, Germany*

[3]*Institute for Theoretical Physics, University of Bremen, Otto-Hahn-Allee 1, 28359 Bremen, Germany and*

[4]*Centre for Quantum Technologies, National University of Singapore, 3 Science Drive 2, Singapore 117543*

EQUILIBRIUM PHASE DIAGRAM OF THE TWO-RUNG TRIANGULAR HUBBARD HAMILTONIAN

Here we identify the key properties of the different phases of the Hamiltonian

$$H(t) = -\tau(t) \sum_{ij\in\langle n.n\rangle,\sigma} (c^\dagger_{\sigma,i} c_{\sigma,j} + \text{h.c}) \; - \tau' \sum_{ij\in\langle \text{vert}\rangle,\sigma} (c^\dagger_{\sigma,i} c_{\sigma,j} + \text{h.c}) + U(t) \sum_i n_{i,\uparrow} n_{i,\downarrow}. \tag{1}$$

A description of the various terms and the lattice geometry are provided in the main text. For convenience, we refer to the outer sites of the ladder as sub-lattice A and the central sites as sub-lattice B - these correspond to the blue and grey sites in Fig. 1 (top left) respectively. We also define the vertical hopping term H_V as

$$H_V = - \sum_{ij\in\langle \text{vert}\rangle,\sigma} (c^\dagger_{\sigma,i} c_{\sigma,j} + \text{h.c}). \tag{2}$$

Firstly, we explore the properties of the ground state of $H(0)$, with $\bar{U} = U(0)$ and $\bar{\tau} = \tau(0)$ being the equilibrium values of the nearest-neighbour hopping and interaction strengths. In the top row of Fig 1, for a range of $\bar{U}$ and τ', we reproduce the phase diagram from the main text as a function of $\langle S^+ S^- \rangle$. We have also provided a diagram of the geometry of the system here, with the numbers indicating the manner in which sites are indexed. In the remainder of the figure we plot the spin-exchange and magnetic order, as well as the corresponding structure factors, for the 3 different phases. The relevant operators for computing these matrices are

$$S^z_i = n_{\uparrow,i} - n_{\downarrow,i}, \qquad S^+_i = c^\dagger_{i,\uparrow} c_{i,\downarrow}, \qquad S^-_i = c^\dagger_{i,\downarrow} c_{i,\uparrow}, \tag{3}$$

and the corresponding structure factors are defined as

$$S_\pm(q) = \sum_{jk} e^{i(j-k)q} \langle S^+_j S^-_k \rangle, \qquad S_z(q) = \sum_{jk} e^{i(j-k)q} \langle S^z_j S^z_k \rangle, \tag{4}$$

where q ranges in discrete steps of $(2\pi/L)$ from $-\pi$ to π.

Within phase I, the system is similar to that of a Spin-Wave Condensate (SWC). Here, there is long-range spin-exchange order throughout the system which does not decay with distance and this leads to the large value of $\langle S^+S^-\rangle$ within this phase. Within sub-lattice A (blue sites in top left of Fig. 1) this order is positive and completely uniform with distance. This order leads to a single structure factor peak at $q = 0$, which indicates the presence of a robust spin-wave condensate. When considering the whole system, however, there is a staggered pattern in the spin-exchange correlations and two additional peaks of opposite momenta in the structure factor appear. This shows there is an interference pattern in the spin-exchange order due to the correlations between the two sub-lattices. This interference co-exists with the condensate.

As τ' increases the system transitions into phase II. Here, τ' is strong enough to break up the condensate and some of the vertically bonded pairs of sites become asymmetric singlets unbound from the rest of the lattice. This is indicated by the formation of a small dip at $\delta = 1$ in the magnetic and spin-exchange correlations in sub-lattice A. The remaining sites still retain some of the correlations seen in phase I, however these decay with distance and the 0 momenta peak in the spin-exchange structure factor has been depleted.

Finally, for large enough τ' the system resides in a spin-dimerized phase (phase III) where all the vertically bonded sites form asymmetric singlets unentangled with the rest of the system. These can be seen in the sharp dip at $\delta = 1$ in both the spin-exchange and magnetic correlations. There is no long-range order in any part of the system, and all the fermions have become localised.

In Fig. 2 we consider how the properties of these states changes with system size in order to classify the transitions observed in the phase diagram of Fig. 1. We restrict ourselves to $U = 5.0\bar{\tau}$ and note that the discontinuous behaviour we observe appears for a range of U, with the critical values of τ' dependent on the explicit value of U. For $U = 5.0\bar{\tau}$ we observe 3 key critical points at $\tau' \approx 0.69\bar{\tau}, 0.86\bar{\tau}$ and $1.35\bar{\tau}$, where discontinuities appear in a number of observables: the derivative of the energy per site with respect to τ', the average number of doublons in the system and the total normalised spin-exchange order $\langle S^+S^-\rangle/L^2$. These discontinuities appear for all the system sizes we consider and thus point to the possible existence of several first-order phase transitions.

As the system size increases we observe that the size of the first discontinuity at $\tau' \approx 0.69\bar{\tau}$ is diminishing towards 0 whilst the other two appear to be stable/ increasing. Hence, in the thermodynamic limit the two points $0.86\bar{\tau}$ and $1.35\bar{\tau}$ correspond to first-order phase transitions between the different phases previously identified: for $\tau' < 0.86\bar{\tau}$ the system is in phase I consistent with the finite value of $\lim_{L\to\infty}\langle S^+S^-\rangle/(L^2) = 1/36$ which was obtained by finding exact polynomials for the scaling of $\langle S^+S^-\rangle$ with system size. For $0.86\bar{\tau} < \tau' < 1.35\bar{\tau}$ the system is in phase II and for $\tau' > 1.35\bar{\tau}$ the system is in phase III.

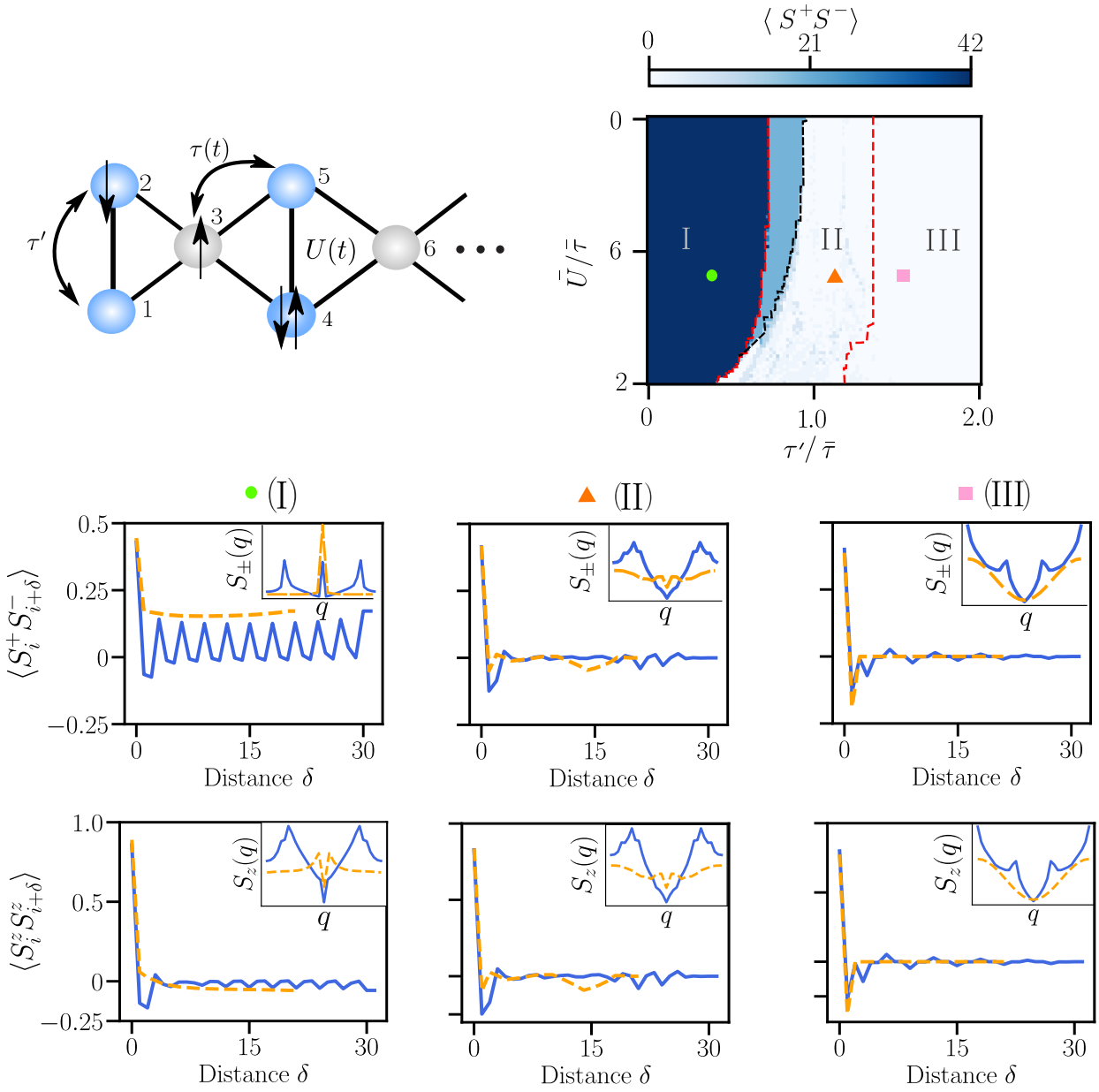

FIG. 1. Top Row) Reproduced from Fig.1 and Fig. 3b of the main text. Left - Geometry of the two-rung Hubbard model described by Eq. (1). The numbers indicate the indexing of the sites, with the blue and grey sites corresponding to sub-lattices A and B respectively. Right - Expectation value of $\langle S^+S^- \rangle$ for the ground state of the $L = 32$ two-rung triangular Hubbard model, see Eq. (1), as a function of $\bar{U}$ and τ'. The *red* dotted lines separate the three distinct phases/regions - I, II and III - observed for this system size, their properties are described in the text. In the thermodynamic limit the width of region I changes and the I - II transition instead occurs along the *black* dotted line. Second and Third Rows) Respectively, spin-exchange and magnetic correlations versus distance δ. Insets) Spin-exchange and magnetic structure factors, see Eq. (4), versus quasi-momenta q. Orange-dotted lines show the corresponding quantities when calculated solely over sub-lattice A, which corresponds to the blue sites in the lattice depicted in the top left plot.

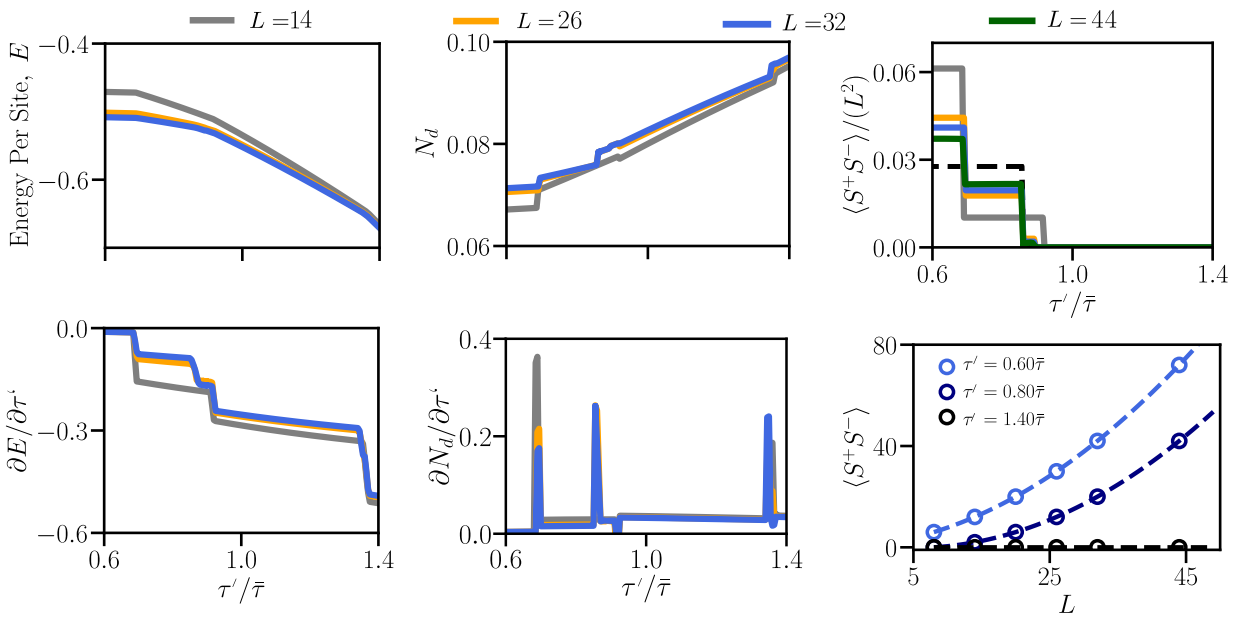

FIG. 2. Top Row) Energy per site, average doublon occupancy N_d and spin-exchange order parameter verus τ' for the ground state of the two-rung triangular Hubbard model described in (Eq. 1) with $U = 5.0\bar{\tau}$. Several system sizes are plotted (the legend is provided above the plots) and the black dotted line in the top right plot is an extrapolation to the thermodynamic limit. Bottom Row) Left and Middle - Derivatives of the Energy per site and average doublon occupancy with respect to τ'. Right - Scaling of $\langle S^+S^-\rangle$ with L for several τ'. Dotted Lines correspond to the polynomials $\langle S^+S^-\rangle = L^2/36 + 7L/18 + 10/9$, $\langle S^+S^-\rangle = L^2/36 - 5L/18 + 4/9$ and $\langle S^+S^-\rangle = 0$ for the respective τ'. These polynomials have been used to determine the value of $\langle S^+S^-\rangle/L^2$ in the thermodynamic limit.

We note that the value of the transition between phases I and II in the thermodynamic limit is distinct from that observed in the finite size calculations. For example, for $L = 14$ we observe this transition at $0.69\bar{\tau}$, where the condensate order first exhibits a discontinuity and we observe a critical change in the system's behaviour under driving (Fig. 2 of the main text). This distinction appears because as the system size increases the condensate order parameter in the region $0.69\bar{\tau} < \tau' < 0.86\bar{\tau}$ increases from 0 (for $L = 8$) and approaches that of the phase I. This region is approximately covered by the light blue area of the phase diagram in Fig. 1. This suggests that in the thermodynamic limit the critical change in the system's dynamics under driving should occur at $\tau' \approx 0.86\bar{\tau}$, where the condensate order jumps to 0 (top right, Fig. 2). Hence, the driving can only induce long-range doublon-holon order for $\tau' < 0.86\bar{\tau}$.

NON-EQUILIBRIUM BEHAVIOUR OF THE TWO-RUNG TRIANGULAR HUBBARD HAMILTONIAN

In Figs. 3 and 4 we concern ourselves with the effect of $H(t)$ when dynamically evolving the phases discussed in the previous section. Specifically, we focus on the role of the vertical hopping integral H_V and how it affects the conservation of $\langle \eta^+ \eta^- \rangle$ as the system absorbs energy from the driving.

Firstly, in Fig. 3, we see that within the phase I H_V effectively annihilates the ground state. This can be understood from its spin-wave condensed nature and the fact the vertical hopping integral acts between sites solely within sub-lattice A (blue sites in top right of Fig. 1). Within this sub-lattice the spin-exchange correlations are large, positive and completely uniform with distance and in Fig. 3 we see that the two-site reduced density matrix (RDM) in this region is approximately of the form

$$\rho \approx \rho' = c_1(|\uparrow,\uparrow\rangle\langle\uparrow,\uparrow| + |\downarrow,\downarrow\rangle\langle\downarrow,\downarrow|) + c_2(\big(|\uparrow,\downarrow\rangle + |\downarrow,\uparrow\rangle\big)\big(\langle\uparrow,\downarrow| + \langle\downarrow,\uparrow|\big)) \tag{5}$$

where c_1 and c_2 are constants which are an order of magnitude larger than any of the other matrix elements in ρ. The term $c_2\big(|\uparrow,\downarrow\rangle + |\downarrow,\uparrow\rangle\big)\big(\langle\uparrow,\downarrow| + \langle\downarrow,\uparrow|\big)$ is the cause of the large spin-exchange correlations and it is straightforward to see that ρ' (and thus approximately ρ) is annihilated by a Hubbard hopping operator acting from either the left or the right. Moreover, ρ' is exactly that one obtains when taking the two-site RDM of the spin-wave condensate $(S^+)^{X/2}\,|\downarrow_1\downarrow_2 \ldots \downarrow_X\rangle$ for any lattice with X sites. Hence, the annihilative action of H_V in region I is a direct result of the spin-wave nature of the ground-state in sub-lattice A.

Meanwhile in the other two phases the ground state is no longer annihilated by H_V. In fact we can see that from the reduced density matrix the vertically bonded sites form a state with strong asymmetric singlet correlations, which a hopping term will have a significant effect on (hopping terms map anti-symmetric singlets onto an orthogonal state with an identical norm).

These observations are reflected in Fig. 4 where we time evolve the ground state under $H(t)$ for various different driving parameters. We see that $\langle \eta^+ \eta^- \rangle$ is effectively unchanged in phase I which can be understood from the annihilative action of H_V - this is no longer true in the other phases where $\langle \eta^+ \eta^- \rangle$ is clearly not conserved.

Although H_V acts as an annihilation operator on the ground state and $\langle \eta^+ \eta^- \rangle$ should therefore be conserved on a very short time-scale, one could argue that this will no longer be the case after a reasonable period of time as the driving will have caused a significant change in the initial wavefunction. This is not what we observe and in Fig. 2 of the main text we see that H_V acts as an annihilation operator over fairly long periods of time, resulting in the approximate conservation of $\langle \eta^+ \eta^- \rangle$ and the build up of doublon-holon order. We understand this from the fact that, transiently, driving at the frequencies and amplitudes

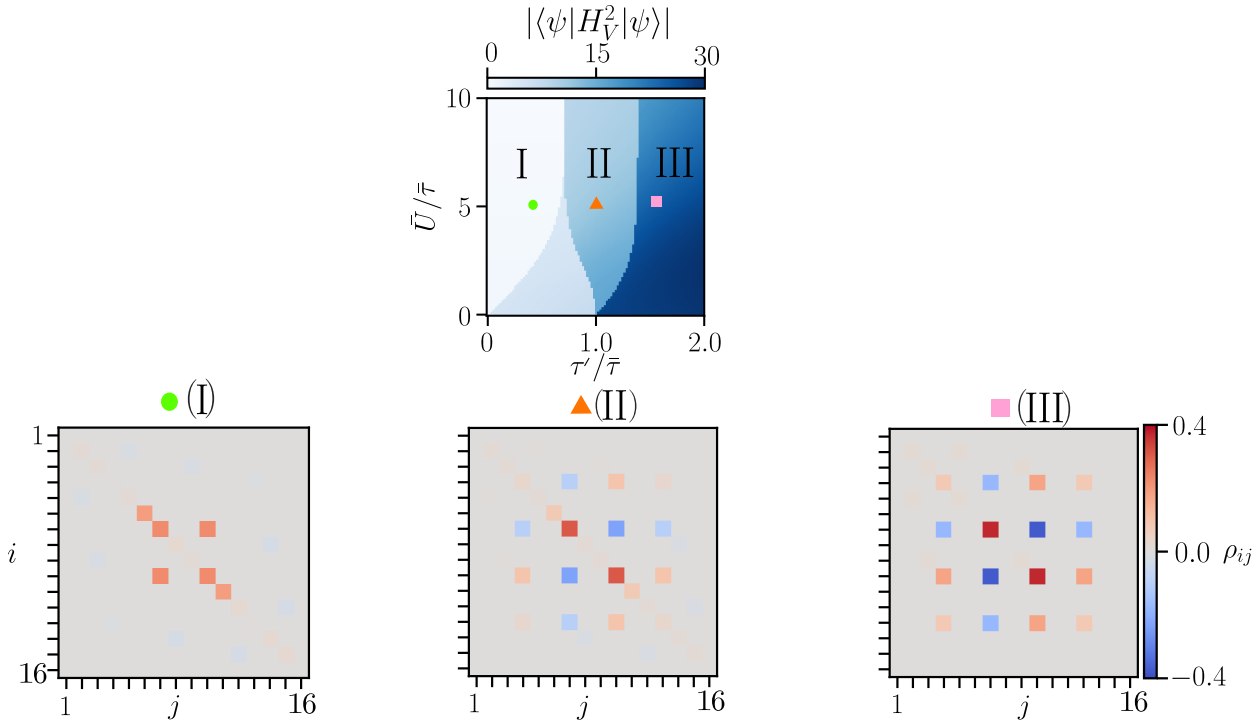

FIG. 3. Ground State Properties of the $L = 8$-site two-rung triangular Hubbard model described in Eq. (1). Top row) Expectation value of the square of the vertical hopping integral, H_V, for a given $\bar{U}$ and τ'. Second row) Average reduced density matrix for a pair of vertically bonded sites. We have used $U = 5.0\bar{\tau}$ and $\tau' = 0.5, 1.0$ and $1.5\bar{\tau}$ respectively. The indices i and j run through the different basis vectors with $|\uparrow\downarrow,\uparrow\downarrow\rangle$ corresponding to $i = 1$. The second quantum number changes each time the index increases by 1 in the cyclic order $|\uparrow\downarrow\rangle \to |\uparrow\rangle \to |\downarrow\rangle \to |0\rangle \to |\uparrow\downarrow\rangle \ldots$ and the first quantum number changes, in the same order, every fourth increment.

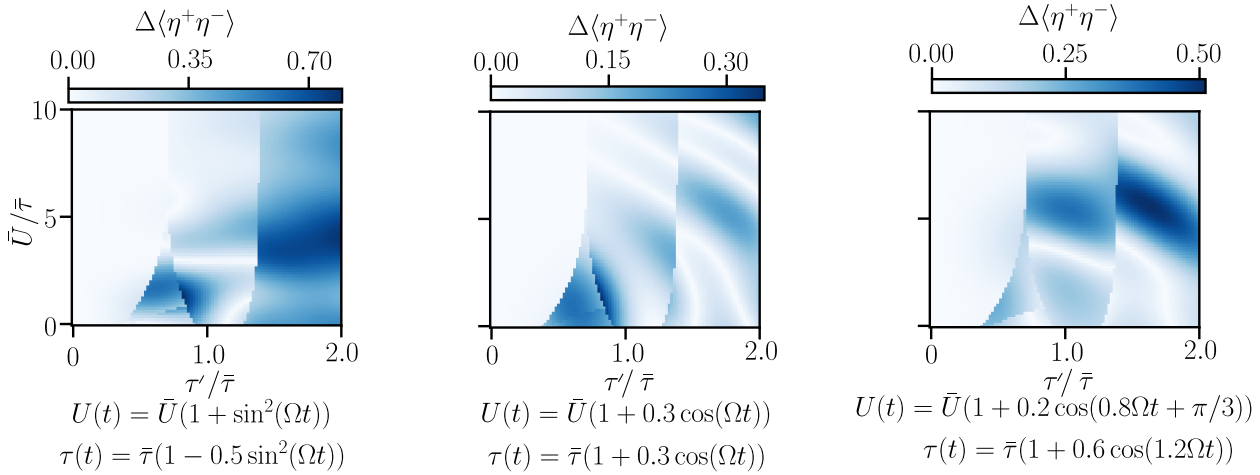

FIG. 4. Change in $\langle\eta^+\eta^-\rangle$ after time-evolving the ground state of the $L = 8$ two-site triangular Hubbard model under $H(t)$ (see Eq. (1)) with the specified $\bar{U}$ and τ'. Each plot corresponds to a different time-dependence of the interaction strength and first hopping integral. We fix $\Omega = 2.25\bar{\tau}$ and calculate $\Delta\langle\eta^+\eta^-\rangle = \langle\eta^+\eta^-\rangle(t_f) - \langle\eta^+\eta^-\rangle(0)$, where $t_f\bar{\tau} = 2.0$

we use in the main text mainly causes changes in the longer-range correlations in the system - as opposed to more local, nearest-neighbour correlations. This can be seen in Fig. 5, where we compare the effect of two different driving frequencies on the correlations in the system. As a result the two-site RDM for a vertically bonded pair of sites stays close to that observed in Fig. 3 and H_V transiently annihilates the non-equilibrium state when driving from within the phase I.

DIABATIC BEHAVIOUR WHEN DRIVING AT LARGE FREQUENCIES

In Fig. 5 we plot the dynamics of the particle-hole correlations at various distances for two different driving frequencies, with the form of the driving now the same as in the main text

$$\tau(t) = \bar{\tau}\big(1 + A_1 \sin^2(\Omega t) \exp\big(-(t-T_p)^2/(2T_w^2)\big)\big),$$
$$U(t) = \bar{U}\big(1 + A_2 \sin^2(\Omega t) \exp\big(-(t-T_p)^2/(2T_w^2)\big)\big). \tag{6}$$

The two frequencies we consider correspond to the two peaks of the distributions in Fig. 4 of the main text. We see that at the higher frequency, the driving induces a much stronger change in the short-range correlations as opposed to the longer-range correlations. The opposite occurs at the lower frequency. This is a consequence of, at the higher frequency, the driving frequency being the largest timescale in the system. As a result a 'freezing effect' occurs where the system struggles to adapt its spatial configuration and the driving induces a more local response in the system's dynamics [1, 2].

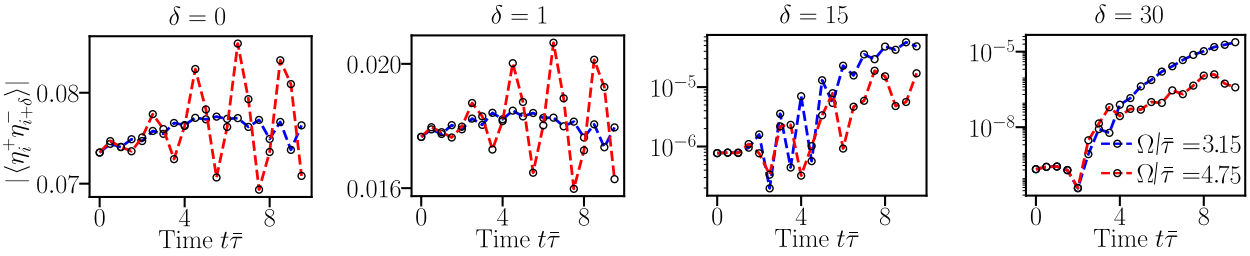

FIG. 5. Simulation of the half-filled driven $L = 32$ triangular Hubbard model in Eq. (1). The system is initialized in the ground state of $H(0)$, setting $\bar{U} = 4.82\bar{\tau}$ and $\tau' = 0.25\bar{\tau}$. The system is then time evolved under $H(t)$, using the same $\bar{U}$ and τ' and setting $A_1 = -0.15, A_2 = -0.075, T_w = 2.5\tau(0), T_p = 5.0\tau(0)$ and Ω to the specified frequency (red, $\Omega/\bar{\tau} = 3.25$, blue $\Omega/\bar{\tau} = 4.75$). These frequencies corresponds to the peaks of Figs 4 in the main text. Here we plot the time evolution of the average magnitude of the particle-hole correlations at distances $\delta = 0, 1, 15, 30$ respectively. For $\delta = 0$ this corresponds to the on-site doublon density. For $\delta = 15$ and $\delta = 30$ the y=axis is plotted on a logarithmic scale.

[1] M. Bukov, L. D'Alessio, and A. Polkovnikov. Universal high-frequency behavior of periodically driven systems: from dynamical stabilization to floquet engineering. *Advances in Physics*, 64(2):139–226, 2015. doi: 10.1080/00018732.2015.1055918.

[2] J. R. Coulthard, S. R. Clark, S. Al-Assam, A. Cavalleri, and D. Jaksch. Enhancement of superexchange pairing in the periodically driven hubbard model. *Phys. Rev. B*, 96:085104, Aug 2017. doi:10.1103/PhysRevB.96.085104.